CRYSTAL GROWTH & DESIGN



pubs.acs.org/crystal
Article

# Solvent Isotope Effects in Protein Adsorption and Crystallization

Hadra Banks, Christian Beck, Cara Buchholz, Simon Christmann, Furio Surfaro, Alexander Gerlach, and Frank Schreiber*

Cite This: *Cryst. Growth Des.* 2025, 25, 5174−5182
Read Online





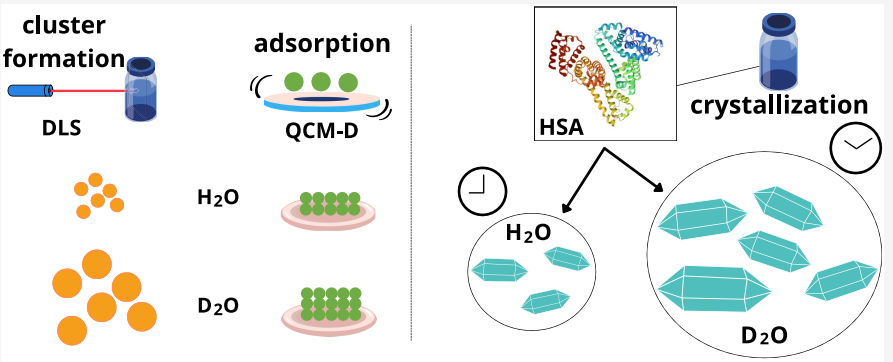


**ABSTRACT:** We investigate the effects of $D_2O$ (heavy water) versus $H_2O$ (normal water) on protein adsorption and crystallization using human serum albumin (HSA) as a model protein in the presence of lanthanum chloride ($LaCl_3$). We use optical microscopy to investigate the crystallization, quartz crystal microbalance with dissipation monitoring (QCM-D) to follow protein adsorption, and dynamic light scattering (DLS) to study cluster formation prior to crystallization. The results show that $D_2O$ induces a higher crystallization density (number of crystals) and the formation of larger crystals; furthermore, $D_2O$ significantly slows down the crystallization kinetics. HSA adsorbs more mass at the surface when the solvent is heavy water, which contributes to the higher crystallization density. Additionally, we find that in heavy water, larger clusters are stabilized prior to crystal growth, which delays the kinetics of crystallization. We speculate that this is due to the modified effective solvent interactions.

## 1. INTRODUCTION

Protein crystallization is a crucial process in a variety of fields as diverse as structural biology, pharmaceutical sciences and the food industry.[1,2] Also, solving protein structures is essential for understanding protein function. The main technique used for this purpose is X-ray crystallography, which requires high-quality protein crystals.[3−6] However, not all proteins have been successfully crystallized, mostly due to limited understanding of the protein crystallization process.[1] Understanding the factors that affect crystallization can help to optimize the conditions.[7−9] Key points are the tuning of the solution's composition and the resulting intermolecular forces.[10−12] A rather subtle factor in this context is the nature of the solvent and its isotope composition, such as the replacement of normal water ($H_2O$) by heavy water ($D_2O$) and the associated change of the effective interactions.

Heavy water is routinely used as an "equivalent" replacement for normal water in protein research, partly due to the need for the deuterium isotope in experimental techniques such as neutron scattering, infrared spectroscopy, and nuclear magnetic resonance.[13−16] However, in recent years, it has become evident that using $D_2O$ as a solvent, compared to $H_2O$, can alter protein behavior, and it cannot be considered a strictly equivalent substitute.[15,17−21] Therefore, in addition to the interest in heavy water for protein crystallization, it is also important for other practical applications to consider the effects of $D_2O$ on protein behavior.

Here, we investigate the effects of deuterium oxide ($D_2O$) on protein adsorption and crystallization, compared to $H_2O$. As a protein crystallization model system, we use the negatively charged globular protein human serum albumin (HSA), the most abundant blood protein, with blood plasma concentrations varying from 35 up to 55 mg/mL.[22,23] To induce nucleation and crystal growth, we use the trivalent salt lanthanum chloride ($LaCl_3$), as in the presence of trivalent salts, HSA crystallizes with a defined crystal structure. It has been shown that the system HSA−$LaCl_3$ can be modeled by an ion-activated mechanism for patchy interaction.[24,25] The interaction is ligand-specific, where the trivalent salt binds

Received: January 28, 2025
Revised: June 20, 2025
Accepted: June 23, 2025
Published: June 27, 2025

into the protein molecule and creates a bridge with another protein molecule, mediating the interaction and triggering several processes such as liquid−liquid phase separation (LLPS), aggregation, crystallization, and enhanced adsorption.[26−32] In a previous study, we found that HSA in the presence of $LaCl_3$ in $H_2O$ crystallizes at the surface after enhanced adsorption.[33]

Below, we show that HSA in the presence of $LaCl_3$ in $D_2O$ behaves qualitatively similarly but with some significant differences. We first address the differences in the crystallization behavior of HSA in water and in heavy water using optical microscopy and a kinetic model. As the interface can be very relevant to protein crystallization, we investigate protein adsorption using a quartz crystal microbalance with dissipation monitoring (QCM-D), and finally, we analyze the diffusion of HSA with Dynamic Light Scattering (DLS). Based on our findings, we hypothesize that the higher local supersaturation at the surface increases the crystallization density and crystal sizes in the presence of heavy water. Additionally, we hypothesize that the significantly slowed crystallization kinetics in $D_2O$ is related to the stabilization of larger clusters prior to nucleation and crystal growth.

## 2. RESULTS

**2.1. Protein−Protein Interactions.** HSA in solution is negatively charged at a neutral pH,[26,34,35] and the protein molecules repel each other. With the addition of the trivalent salt $LaCl_3$, protein−protein interactions are gradually becoming more attractive with the increase of the salt concentration ($c_s$). The phase boundaries of the HSA−$LaCl_3$ solution were investigated for $c_p$ above 40 up to 85 mg/mL, and samples were prepared and immediately analyzed. In the phase diagram (Figure 1) the region where repulsive interactions are still dominant is located below phase boundary $c^*$. The value $c^*$ is the concentration of salt, at a given protein concentration ($c_p$) where the solution becomes visibly turbid, marking the beginning of a phase diagram region dominated by attractive protein−protein interactions.[12] The specific $c^*$ value of HSA in the presence of $H_2O$ or $D_2O$ is similar but slightly shifted. At $c_p$ = 50 mg/mL, the phase boundary value ($c^*$) is 2.8 mM in normal water and 2.3 mM in heavy water, see Table S1 for additional $c^*$ values. This is in agreement with ref 18, where the authors find a shifted phase diagram in a similar system (bovine serum albumin with $LaCl_3$). In this study, they also found that near $c^*$, the protein interactions are different in heavy water and in normal water.

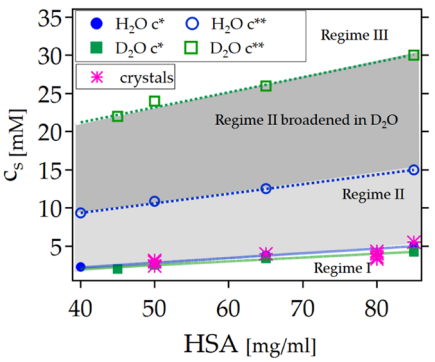


**Figure 1.** Phase diagram of HSA in the presence of $LaCl_3$ in $D_2O$ (green squares) and in $H_2O$ (blue circles). In Regime I and III, the solution is visibly clear, while in Regime II, the solution is turbid due to attractive interactions. The $c^*$ value is similar for both solvents; however, the $c^{**}$ value is significantly different, resulting in a broadening of the attractive regime in heavy water.

Upon further increase of the trivalent salt $c_s$, a second-phase boundary is crossed ($c^{**}$), where a charge inversion at the surface of proteins occurs as a result of screening cations (specific values are shown in Table S1). Above $c^{**}$, repulsive interactions are dominant, and the solution is visibly clear. This phenomenon is called re-entrant condensation.[12,29]

The first striking difference between both solvents is the $c^{**}$ value, which leads to a broadening of the attractive regime in the phase diagram of HSA in a heavy water solution. The salt concentration for re-entrant condensation to occur has to be much higher in $D_2O$ compared to $H_2O$.

Here, experiments were performed at a fixed protein and salt concentration (Figure 1), and experiments on the kinetics were also performed at a fixed phase diagram location (same distance to the $c^*$ value). The conditions chosen for all experiments are in a relatively narrow region, near the phase boundary $c^*$, and exhibit similar salt-to-protein ratios (Figure 1). As a result, they have similar effective protein−protein interactions.[18,36]

**2.2. Crystallization.** HSA is known to crystallize in the presence of trivalent salts.[26−28,33,37] Here, we use HSA in the presence of $LaCl_3$ as a model system to investigate the effect of solvent isotope on protein crystallization. A batch method was employed to measure crystal density, crystal size, and crystallization kinetics of HSA with $LaCl_3$ on a glass slide. For typical conditions, we find that the crystallization density (number of crystals per area) is higher in $D_2O$, see Figure 2a. The data show that the absolute number of crystals is about twice as high in $D_2O$ than in $H_2O$. The experiment was repeated with three different HSA batches; error bars account for the batch-to-batch variation. In all batches, the crystallization density is higher in heavy water. Additional measure-

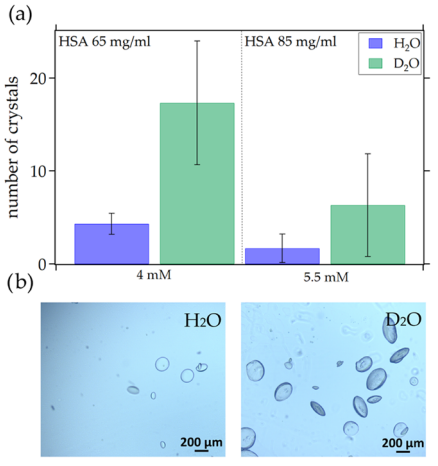


**Figure 2.** HSA crystallization in the presence of $LaCl_3$, in heavy water or normal water. (a) Crystallization density (number of crystals per area) at the end of the observation period. For both protein concentrations, there are more crystals in heavy water. (b) Microscopy images showing the general crystal morphology, both present a lentil-like shape. The protein concentration is 80 mg/mL and salt concentration for normal water 4.3 mM and heavy water 3.3 mM. The images were taken after 15 days of sample preparation (kept at room temperature). For a three-dimensional (3D) view of the crystals attached to the surface, we refer to ref 33.



https://doi.org/10.1021/acs.cgd.5c00116
Cryst. Growth Des. 2025, 25, 5174−5182

ments are shown in the Supporting Information (Figure S1). Furthermore, we find that crystals grow to larger sizes in heavy water. The largest crystal observed in heavy water ($c_p$ = 65 mg/mL; $c_s$ = 4 mM) measured 561 $\mu$m, whereas in normal water under the same conditions, the largest crystal was 256 $\mu$m. A distribution of the measured crystal lengths is presented in the Supporting Information (Figure S2). The aspect ratio of the crystal was comparable for both solvents, namely a lentil-like shape (Figure 2b).[33]

Crystallization density is not the only difference observed here. The different kinetics of crystallization (see Figure 3)

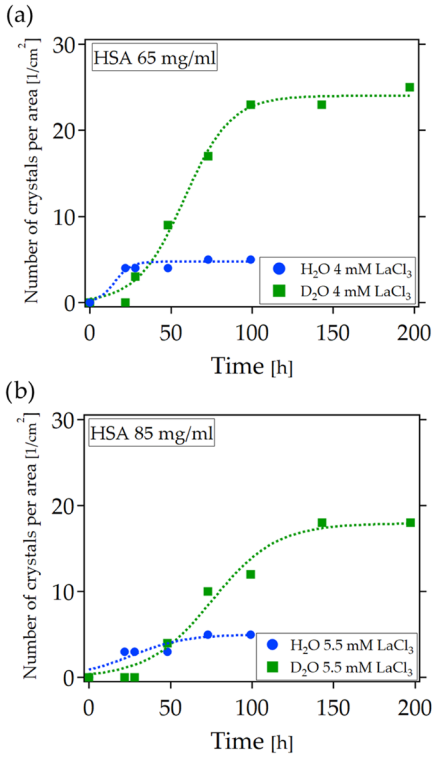


**Figure 3.** Number of crystals per area under the same conditions, over time, fitted with a sigmoidal function (see eq 2), for $D_2O$ (green squares) and $H_2O$ (blue circles). In heavy water, the nucleation takes longer but the total number of crystals is finally bigger.

clearly show the impact of the solvent. We utilized a kinetic model derived from the sigmoidal model of nucleation rate.[28,38] This model describes the temporal evolution of the number of nuclei ($N(t)$) as the result of two key contributions: the first term below represents the rate at which nuclei are formed, while the second term accounts for their consumption. The overall expression is given by

$$\frac{dN}{dt} = kN - k\frac{N^2}{N_s} = kN\left(1 - \frac{N}{N_s}\right) \quad (1)$$

Here, $N_s$ represents the number of nuclei at saturation. The preceding equation is a first-order differential equation that can be solved analytically to derive an expression suitable for fitting the experimental data from the nucleation density plot. This plot is generated by daily counting the number of crystals on glass slides using an optical microscope. Upon solving the differential equation, the final sigmoidal expression for the nuclei formation is given by

$$N(t) = \frac{N_s}{1 + \exp(-k(t - t_c))} \quad (2)$$

From this, the nucleation rate $k$, and the critical nucleation time $t_c$ defined as the time when half of the nuclei have formed, can be determined.

We observe a slight increase in the number of crystals after several days due to minor secondary nucleation (a few small crystals growing at the end of crystallization). As a result, the fitted curve may reach saturation slightly earlier than the experimental data. Crystallization occurs later for the heavy water solution, which is reflected by higher values of the incubation parameter $t_c$ in $D_2O$ (see Table 1).

**Table 1. Induction Time ($t_c$) of HSA Crystallization in Heavy Water and Normal Water**

| $c_p$ (mg/mL) | $c_s$ (mM) | solvent | $t_c$ (h) |
|---|---|---|---|
| 50 | 2.9 | $H_2O$ | 41.7 |
| 50 | 2.4 | $D_2O$ | 111.5 |
| 65 | 4 | $H_2O$ | 15.3 |
| 65 | 4 | $D_2O$ | 58 |
| 80 | 4 | $H_2O$ | 15.6 |
| 80 | 3.6 | $D_2O$ | 89.7 |
| 85 | 5.5 | $H_2O$ | 25.3 |
| 85 | 5.5 | $D_2O$ | 75.5 |

To further investigate the kinetics, two protein concentrations were measured at a fixed location in the phase diagram (Figure 4). For HSA $c_p$ = 50 mg/mL, the $c^*$ is 2.8 mM in normal water and 2.3 mM in heavy water and $c_s$ was chosen at the same distance as the respective $c^*$ values. This was done to understand if the differences in the crystallization behavior arise solely from solvent isotope effects and not from slightly

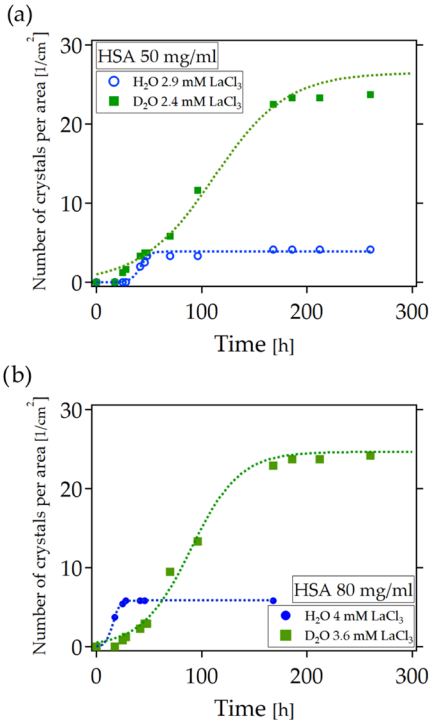


**Figure 4.** Kinetics of protein crystallization, showing the number of crystals per area measured at fixed locations in the phase diagram.



https://doi.org/10.1021/acs.cgd.5c00116
Cryst. Growth Des. 2025, 25, 5174−5182

shifted phase boundaries (as shown in Figure 1). For HSA $c_p$ = 80 mg/mL (Figure 4b), the same consideration was used and the trend observed was confirmed. We find that the kinetics is slowed in heavy water for all conditions tested (Table 1). Notably, we limit the discussion of the data presented in Table 1 to the comparison of $H_2O$ and $D_2O$. It is important to recognize that HSA crystallization is not a simple function of salt and protein concentration, as demonstrated in ref 28. Here, we provide several data points near the phase boundary concentration for each solvent, allowing for a better comparison of the crystallization behavior between $H_2O$ and $D_2O$.

In summary, the crystallization behavior is significantly different, highlighting the importance of the solvent isotope effect on the crystallization of proteins. While the crystallization density is higher in $D_2O$ (Figure 2), the kinetics is consistently slower (Figures 3 and 4). Nucleation takes longer to occur in heavy water (Table 1), but more and bigger crystals are forming. According to ref 15, some protein systems exhibit accelerated assembly kinetics in heavy water compared to normal water, while others exhibit slowed kinetics. Therefore, the higher viscosity of $D_2O$[39] may not be the only factor contributing to the slowed-down kinetics observed in our protein−salt system. To address this issue, we investigated the key factors that are involved in protein crystallization, starting with the protein−surface interaction.

**2.3. Adsorption.** As the crystallization of this system in normal water tends to be surface-assisted,[33] the first step in understanding the reasons behind the solvent differences observed is to investigate the protein−surface interaction.

In the QCM-D technique, a larger frequency shift is correlated to a higher adsorbed mass, as described by the Sauerbrey equation.[40] In Figure 5, the seventh harmonic ($\Delta f_7$) was chosen to compare the adsorption of HSA ($c_p$ = 65 mg/mL) in water with heavy water due to the reliable stability of this harmonic.[41] The data shown in Figure 5a refer to 1 h of adsorption; the sensor surface was then rinsed with water to measure only irreversibly adsorbed proteins. HSA without any addition of salt already shows a different adsorption behavior when changing from $H_2O$ to $D_2O$. Increasing the salt concentration, the difference in the frequency shift remains nearly constant. We found that the protein−surface interaction is stronger in $D_2O$ compared to $H_2O$, as in normal water, the proteins are easier to rinse off, leaving a lower adsorbed mass attached to the surface.

To assess the amounts of reversibly and irreversibly adsorbed proteins, we measured protein adsorption after 15 h of contact between the solution and the surface without rinsing the surface. A clear difference between the frequency shift is visible between heavy and normal water (Figure 5b). We note that with increasing salt concentration, the difference between frequency shifts is more significant, and the adsorption in heavy water is nearly twice that observed when the salt concentration is increased. HSA accumulates more mass at the surface when the solvent is $D_2O$, and this effect is more pronounced with increasing salt concentrations.

QCM-D measures the frequency shift and simultaneously the dissipation of the adsorbed layer. This parameter is associated with the viscoelastic properties of the layer.[42,43] In heavy water, the dissipation is higher, especially at higher salt concentrations, where with $c_s$ = 2.73 mM, the $\Delta D$ is 31 ppm for $D_2O$ and 24 ppm for $H_2O$, which means that the adsorbed layer is softer in $D_2O$.[42]

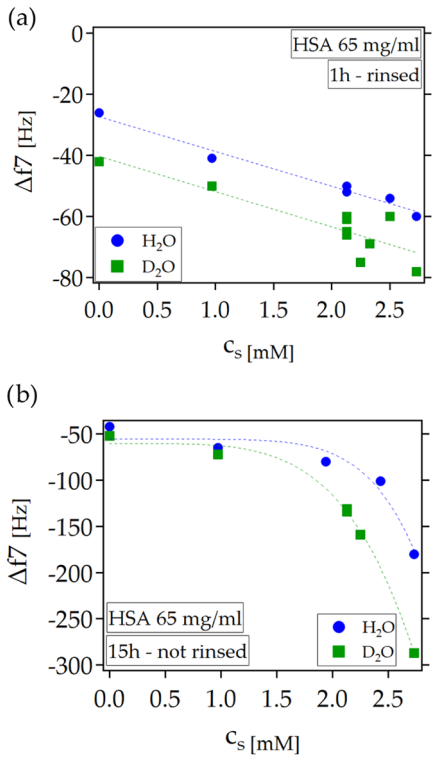


**Figure 5.** Adsorption of a HSA−$LaCl_3$ solution in $D_2O$ (green squares) and $H_2O$ (blue circles) investigated with QCM-D. Frequency shift of HSA $c_p$ = 65 mg/mL and different $c_s$ concentrations (a) rinsed after 1 h to measure irreversibly adsorbed proteins; (b) not rinsed after 15 h of adsorption to measure reversibly and irreversibly adsorbed proteins. Dashed lines are shown to guide the eye.

We have also used the Kelvin−Voigt viscoelastic model to extract the layer thickness (see Section 5.4).[41,43−45] In Table 2 the layer thicknesses are shown for two different salt concentrations. We have chosen zero salt concentration (0 mM) and a low salt concentration (0.97 mM) to ensure that the assumptions in the model are still valid (a homogeneous layer), given that at higher salt concentrations, the adsorbed layer is less homogeneous.[34] The analysis takes into account the higher viscosity and density of liquid $D_2O$ and the higher density of the adsorbed layer in heavy water. The results show that the thickness of the adsorbed layer in $D_2O$ is larger.

**Table 2. Adsorbed Layer Thickness Calculated with the Kelvin−Voigt Viscoelastic Model[41,43−45]**

| $c_p$ (mg/mL) | $c_s$ (mM) | solvent | thickness (nm) |
|---|---|---|---|
| 65 | 0 | $H_2O$ | 6.1 |
| 65 | 0 | $D_2O$ | 10.4 |
| 65 | 0.97 | $H_2O$ | 12.5 |
| 65 | 0.97 | $D_2O$ | 14.7 |

Another difference between the adsorption in the presence of normal or heavy water is the kinetics of the adsorption process. In Figure 6, which shows the frequency shift over time, it is visible that in $H_2O$, the layer saturates faster than in $D_2O$. This shows that the process of adsorption in heavy water continues for a longer time than in normal water, highlighting the importance of measuring the adsorption over many hours to capture the whole adsorption process.



https://doi.org/10.1021/acs.cgd.5c00116
Cryst. Growth Des. 2025, 25, 5174−5182

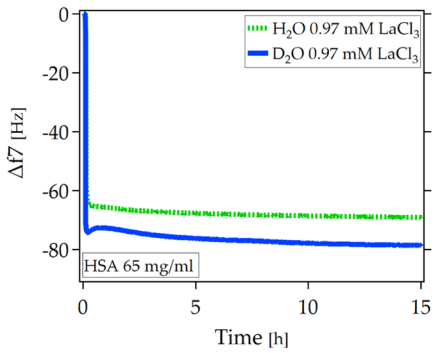


**Figure 6.** Real-time HSA adsorption over 15 h showcasing the slower kinetics until reaching saturation in heavy water.

In summary, we found that a greater amount of HSA adsorbs to the surface when the solvent is $D_2O$ compared to $H_2O$ and that the kinetics is slower, following the same trend observed for the crystallization. The enhanced adsorption in $D_2O$ continues for many hours, forming a thicker layer of proteins. We refer to "enhanced adsorption" as the formation of a thick multilayer over time.[30,31]

**2.4. Diffusion.** To investigate the diffusive properties of the protein solutions, multiangle dynamic light scattering measurements have been performed. With a protein concentration of $c_p$ = 80 mg/mL and a salt concentration of $c_s$ = 4 mM, the sample conditions were chosen to be close to the $c^*$ line (see Figure 1). For both solvents, the correlation functions are characterized by multiple different decays, indicating at least two contributions in the solution as observed previously in similar systems.[10,46−48] The scattering function has been evaluated for each value of scattering vector $q$ with a sum of two exponential functions

$$g_2^n = a\exp(-2\Gamma_1\tau) + (1-a)\exp(-2\Gamma_2\tau) \quad (3)$$

$$g_2^n = \frac{g_2 - 1}{g_2 - 1|_{\tau=0}} \quad (4)$$

with $a$ and $\Gamma_{1,2}$ being the scaling parameter and the decay rates, respectively.

Based on the $q$-dependence of $\Gamma$, the collective long-time diffusion coefficient can be extracted as $\Gamma = Dq^2$. The diffusion coefficients for the monomers and clusters, as well as the scaling parameter at 30°, are displayed for different time steps in Figure 7, and time and angular dependence of the normalized DLS correlation function are shown in Figures S4 and S5 in the Supporting Information. The collective long-time diffusion coefficients are influenced by different parameters such as the interactions between the particles, temperature, particle size, and solvent viscosity. Given the high protein concentrations of the investigated samples, a direct determination of the hydrodynamic radius would require an assumption on the volume fraction influence.[49]

For the analysis of the light scattering data, we therefore focus on the diffusion coefficients as well as scaling parameters. Heavy water has a different viscosity ($\eta$) than normal water; at 20 °C the viscosity of pure $H_2O$ is 1.005 mPa·s, while that of pure $D_2O$ is 1.250 mPa·s.[39] Given that for DLS data analysis, the viscosity must be considered, $D_1$ and $D_2$ were rescaled by the viscosity of the corresponding solvent. For both solvents, an increase of the larger diffusion coefficient $D_2$, which is related to the monomers, is observed, indicating the formation of crystals leading to an inverse crowding effect (Figure 7 top left), as observed previously in other protein crystallization systems.[50] The diffusion coefficients multiplied by the viscosity of the corresponding solvent ($H_2O$ and $D_2O$) result in a comparable value, indicating the presence of monomers in both solutions.

The lower diffusion coefficient $D_1$, shown in Figure 7 bottom left, characterizes the clusters in the solution. For both solvents, the clusters diffuse more than a factor 2 slower than the monomers. In $D_2O$, the diffusion coefficients are smaller

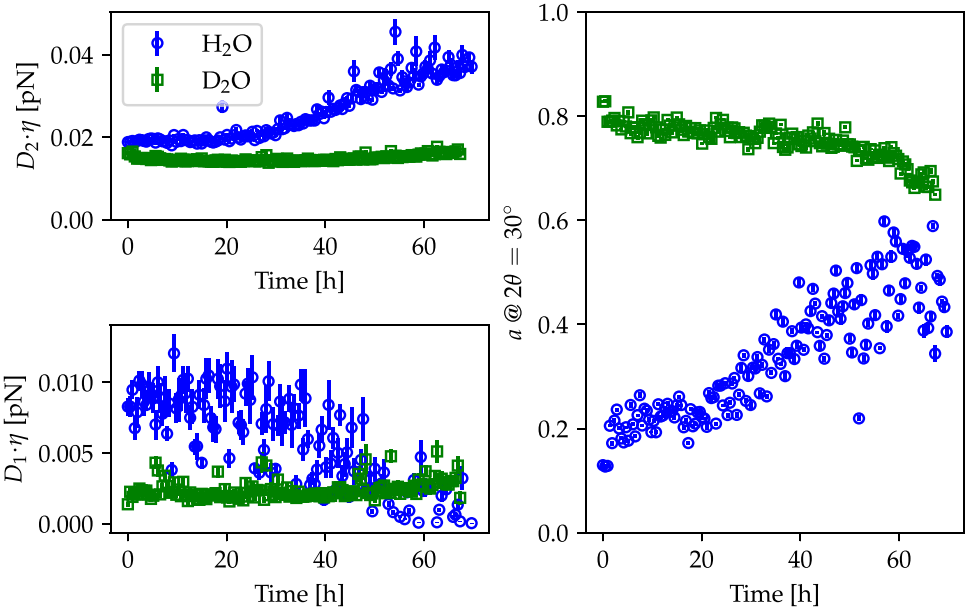


**Figure 7.** Time-dependent DLS results for samples in $H_2O$ (blue circles) and $D_2O$ (green squares). The diffusion coefficients $D_1$ (left bottom describing the protein clusters) and $D_2$ (left top describing the protein monomers) are rescaled by the viscosity of the corresponding solvent. The scaling parameters $a$ from eq 4 are displayed for $2\theta$ = 30° on the right-hand side.



https://doi.org/10.1021/acs.cgd.5c00116
Cryst. Growth Des. 2025, 25, 5174−5182

than in $H_2O$. This indicates the presence of larger clusters in the case of $D_2O$ compared to $H_2O$ directly after the sample preparation.

The crystallization process takes place faster in the case of $H_2O$ resulting in an increase in the cluster size starting at around 30 h. This is visible in the increasing scaling parameter $a$, the decreasing cluster diffusion coefficient $D_1$ as well as the increase of the monomer diffusion coefficient $D_2$ (Figure 7).

## 3. DISCUSSION

We found that the adsorption and crystallization behavior of the HSA−$LaCl_3$ system changes significantly when normal water is replaced with heavy water. Compared to $H_2O$, the crystallization density (number of crystals) is higher in $D_2O$, with larger crystal sizes and slower crystallization kinetics (Figures 2−4). Additionally, the adsorption of HSA at the surface features slower kinetics in heavy water but stronger protein−surface interaction as indicated by the amount of irreversibly adsorbed proteins and a higher total mass at the surface, including both reversible and irreversible adsorption (Figures 5 and 6). The phase diagram also changes, with $D_2O$ requiring a higher critical salt concentration to achieve re-entrant condensation (Figure 1), in agreement with ref 18. Interestingly, our DLS analysis reveals that protein clusters in $D_2O$ are larger from the beginning of the incubation upon salt addition, suggesting that early stabilization of these clusters may slow both the adsorption and crystallization processes of HSA in heavy water (Figure 7).

In ref 15, the authors highlight that protein assemblies exhibit significantly different behaviors when replacing $H_2O$ by $D_2O$. The kinetics of these assemblies can be either sped up or slowed down in heavy water. In ref 51, it is noted that protein assembly kinetics remain unaffected by the different viscosity between these two solvents. Considering that, in the presence of heavy water, assembly rates can vary and that prior studies suggest viscosity is not the main reason for the isotope effect on protein assemblies,[15,19,51−53] we assume that the increased viscosity of $D_2O$ is also not the main factor behind the crystallization and adsorption kinetics observed in our study. Although the different viscosities of the solvents might have an influence, it is not sufficient to explain the different behavior observed here.

This is consistent with our findings, which reveal differences in both the number and size of the crystals (Figure 2). Since HSA in the presence of $LaCl_3$ was shown to crystallize following a surface-assisted mechanism,[33] we discuss the solvent differences considering the protein−surface interaction. The nucleation of crystals at the surface depends on the local protein concentration and the softness of the adsorbed layer.[54] A higher adsorbed mass correlates with a higher supersaturation, and a softer layer allows proteins to rearrange relatively easily into orientations favorable for nucleation and crystal growth (Figure 5).[54,55] In our previous study (ref 33), we found that near the critical salt concentration ($c^*$), HSA adsorption correlates with the crystallization density. In that study, we found that the interface can locally increase the protein concentration due to enhanced adsorption. Proteins first form a monolayer (irreversible adsorption), followed by continued multilayer growth driven by protein−protein attractions. This adsorbed layer locally increases supersaturation, which promotes the nucleation of crystals within the multilayer.[33] For the system HSA with $LaCl_3$, crystals were observed only at the surface, and for the nucleation of crystals to occur, a soft multilayer is needed. Here, a similar behavior is observed: HSA in heavy water yields both more and larger crystals (Figure 2), which correlates with higher adsorbed mass on the surface compared to normal water (Figure 5).

The effects of the interface are also influenced by bulk properties. In the phase diagram of HSA with $LaCl_3$ in the presence of heavy and normal water (Figure 1), we observe a similar critical salt concentration ($c^*$) for both solvents and a significant difference in the second critical salt concentration for re-entrant condensation ($c^{**}$). This is consistent with ref 18, where a similar protein system was investigated and the second virial coefficient ($B_2$) of Bovine Serum Albumin (BSA) with $LaCl_3$ in $H_2O$ and $D_2O$ was determined. The $B_2$ value represents the nature and strength of interaction between protein molecules in solution.[36,56] It is known that $D_2O$ increases attractive protein−protein interactions of many globular proteins in solution compared to $H_2O$,[15,16,18,57] a consequence of which is the broadening of the second regime represented in the phase diagram.[18] Considering adsorption, when the solution comes into contact with the surface, the protein−surface interaction first forms a monolayer of irreversibly adsorbed proteins. Enhanced adsorption then continues for many hours due to protein−protein interactions forming a multilayer, increasing the local protein concentration.[33] The increased protein−protein interactions are the reason for the higher adsorbed mass on the surface (Figure 5).[30,31] This increases the number of the crystals (Figure 2) due to the higher local supersaturation.[58]

The increased protein−protein interactions and adsorption contribute to the higher crystal density observed in heavy water. However, this does not explain the unexpected kinetics, as usually a higher density of crystals is associated with faster kinetics; here, we observe slower kinetics associated with a higher crystal density and size (Figure 2 and Table 1). In our system, the salt bridges the proteins, favoring the formation of clusters, and it is known that these affect pathways of crystallization.[11,27,29] Protein cluster formation is highly sensitive to changes in protein interactions.[11] It has been hypothesized that $D_2O$ stabilizes different intermediates than $H_2O$ due to enhanced hydrophobic effects.[15,51] Our DLS data show that protein clusters in heavy water are larger than those in normal water from the start of the incubation period (immediately after salt addition) (Figure 7). This agrees with the observation that the rate of protein assembly slows down in $D_2O$ if intermediates are involved in the mechanism,[15] such as the formation of an adsorbed layer. We hypothesize that the stabilization of bigger clusters in heavy water (Figure 7) slows down the kinetics of crystallization (Figures 3 and 4), as the first step for crystal nucleation in this system is actually the adsorption of the protein at the surface.[33]

One of the biggest differences between normal water and heavy water is the properties of the hydrogen bonds and their network once the hydrogen is replaced by deuterium.[15] Hydrogen bonds actively contribute to the electrostatic environment of salt bridges,[59] supporting the structural integrity of protein−protein interactions within clusters. In addition, lanthanide ions such as $La^{3+}$ exhibit solvent isotope-dependent hydration properties, including different water exchange dynamics in $D_2O$ compared to $H_2O$, which may further modulate ion-protein binding.[60] Although the exact mechanism for the isotope effect on protein assemblies is not entirely clear,[15,16,18,34,51] this variation in interaction that can



https://doi.org/10.1021/acs.cgd.5c00116
Cryst. Growth Des. 2025, 25, 5174−5182

affect protein clusters may explain the significantly different protein crystallization observed here.

## 4. CONCLUSIONS

In conclusion, we find that isotope substitution from $H_2O$ to $D_2O$ significantly influences the adsorption and crystallization of human serum albumin in the presence of $LaCl_3$. While $D_2O$ increases the crystallization density and crystal size (Figure 2), it unexpectedly slows down the kinetics of both crystallization and adsorption (Figures 3, 4, and 6). We propose that the enhanced stabilization of protein clusters in heavy water slows the kinetics (Figure 7). At the same time, $D_2O$ allows for the formation of more and larger crystals due to the increased protein−protein interactions and adsorption. These findings highlight the complex role of heavy water in tuning protein behavior and the importance of solvent composition in optimizing crystallization conditions.

## 5. METHODS

**5.1. Material and Sample Preparation.** Albumin from human serum (HSA) with a purity ≥97% (A9511) and $LaCl_3$ with a purity of 99.99% (449830) were purchased from Merck. In total, seven different batches were used in this study. Solutions of salt and protein were prepared by dissolution in Milli-Q water or $D_2O$. The concentration of the protein stock solution was determined by UV−vis spectrophotometer measurements (Cary 50 UV−vis spectrometer, Varian Technologies) employing the Lambert−Beer law; the extinction coefficient for HSA is 0.531 mL/(mg·cm), at a wavelength of 278 nm where aromatic amino acids have an absorbance maximum. All samples investigated were prepared by mixing Milli-Q water, protein stock solution, and salt stock solution in vials and immediately used. All experiments were performed in a room with the controlled temperature of 21 ± 1 °C. All concentrations reported (e.g., 50, 80 mg/mL) refer to the final concentration after mixing the protein stock solution, salt solution, and solvent. No buffer was added as neutral trivalent salts (i.e., $LaCl_3$) do not induce significant pH variation.[31,61]

**5.2. Determination of the Phase Diagram.** The phase diagram of HSA with $LaCl_3$ was determined by visual inspection varying the protein $c_p$ and salt concentration $c_s$. Glass vials were used to mix the stock solution of protein with the stock solution of salt, achieving a final volume of 300 μL with the addition of the solvent ($H_2O$ or $D_2O$). At a fixed protein concentration, $LaCl_3$ was added to the solution in a series of samples where the salt concentration was increased until the solution became visibly turbid. The first salt concentration where the solution is visibly turbid is indicated as the first phase boundary ($c^*$). After this turning point, the salt concentration was further increased until the second-phase boundary ($c^{**}$) was reached, where the solution was visibly clear again. The phase boundaries were checked for each protein batch.

**5.3. Crystallization.** Crystallization images were acquired using an optical microscope (Axio Scope.A1, Carl Zeiss AG) and a microscope included a camera (AxioCam ICc5, Carl Zeiss AG) with the software ZEISS ZEN 3.2. The same software was used to process the images.

Batch crystallization experiments for screening crystal density and the crystal size were performed as follows: protein and salt were mixed at different concentrations in an Eppendorf tube, and water was added to achieve the desired volume. A volume of 25 or 65 μL of the freshly mixed solution was placed on a glass slide where spacers made of double-sided adhesive films (Gene Frame, Thermo ScientificTM) were mounted. The area of the spacers is 1 × 1 $cm^2$ for the 25 μL sample and 1.5 × 1.6 $cm^2$ for the 65 μL sample. The solution was then covered with a glass coverslip. The samples were observed with bright-field microscopes in appropriate time intervals, ranging from every few hours to several days. The entire available area within each well was analyzed, and no selection or limitation to a specific region was used. Crystals were counted and imaged with 5 or 10× magnification.

Appropriate conditions were chosen by analyzing the batch method to study the crystallization kinetics. The same method as that described above was used. To analyze the kinetics of the crystallization for the two solvents, the raw data of crystal numbers are fitted with a sigmoidal function (eq 2).

**5.4. Adsorption.** QCM-D is the main technique used in this study to investigate the protein interface behavior. It is a real-time technique that utilizes acoustic waves generated by an oscillating piezoelectric single-crystal quartz plate to analyze surface-interaction phenomena over solid interfaces.

Two different QCM-D instruments were used to investigate protein adsorption, and samples were prepared and analyzed the same way. QCM-D Q-Sense Explorer (Biolin Scientific, Sweden) or QSense Analyzer 4-chamber (Biolin Scientific, Sweden) instruments were used. The QCM-D measurements were acquired and analyzed with software QSoft and Dfind (Biolin Scientific, Sweden), respectively. $SiO_2$-coated flat sensors (5 MHz) (Quantum Design, QS-QSX303, Germany) were used as substrates. For the real-time data presented, the seventh harmonic was chosen due to the good stability that this overtone provides.[41] The experiments were performed as follows: The flow chamber was filled with $H_2O$ or $D_2O$ for calibration and to define a baseline. After recording a stable baseline, the sample was freshly prepared and 400 μL was pumped into the cell containing 100 μL of solution above the sensor. The measurements were done at the controlled temperature of 20 °C. For specific conditions of the 65 mg/mL protein concentration, the experiment was repeated three times. Additional conditions were measured to confirm the observed trend; in total, 41 measurements were performed for each solvent.

The Kelvin−Voigt model[41,43−45] was used to estimate the layer thickness over the surface. The following parameters were used for the model: Bulk layer densities for $D_2O$ (1106 g/L) and $H_2O$ (998 g/L), viscosity of the bulk liquid for $D_2O$ (1.25 mPa·s) and $H_2O$ (1.01 mPa·s), and the adsorbed layer density for $D_2O$ (1250 g/L) and $H_2O$ (1200 g/L). The relationship between QCM-D response and viscoelastic properties of the soft film layer is

$$\Delta f \approx -\frac{1}{2\pi\rho_0 h_0}\left(b + h_1\rho_1\omega - 2h_1 b^2 \frac{\eta_1\omega^2}{\mu_1^2 + \omega^2\eta_1^2}\right)$$

$$\Delta D \approx \frac{1}{\pi f\rho_0 h_0}\left(b + 2h_1 b^2 \frac{\eta_1\omega}{\mu_1^2 + \omega^2\eta_1^2}\right)$$

where $\rho_0$ and $h_0$ are the density and thickness of the quartz; $b$ is equal to $\eta_3/\delta_3$ where $\eta_3$ is the viscosity of the bulk liquid and $\delta_3$ is the viscous penetration depth of the shear wave in the bulk liquid; $\rho_3$ is the density of liquid and $\omega$ the angular frequency of the oscillation. The parameters related to the properties of the adsorbed layer are viscosity ($\eta_1$), thickness ($\delta_1$), shear elasticity ($\mu_1$), and density ($\rho_1$).

**5.5. DLS.** Dynamic light scattering measurements have been performed at room temperature using an ALV/CGS-3 platform-based goniometer system with a HeNe laser. For each angle, five measurements have been performed. Correlation functions were measured with total measurement times of $\tau_{max}$ = 30 s. In Figure 7, the time axis is the kinetic time resulting from the iterative way in which we measured the DLS. The time in Figure 7 is therefore comparable as a parameter to the "time" in Figure 6. Correlation functions have been normalized, dust-contaminated measurements removed, and subsequently averaged. The scattering vector $q$ has been determined by $q = 4\pi n \sin(2\theta/2)\lambda^{-1}$ with a refractive index of $n$ = 1.33. Measurements were performed at scattering angles $2\theta$ = [15, 20, 25, 30, 35, 50, 70, 90, 110, 130, 150°]. Acquisition has been script-based. To avoid changes in protein and salt concentrations, the samples were not filtered before the measurements. Experiments were repeated four times.



https://doi.org/10.1021/acs.cgd.5c00116
Cryst. Growth Des. 2025, 25, 5174−5182

## ■ ASSOCIATED CONTENT

### Supporting Information

The Supporting Information is available free of charge at https://pubs.acs.org/doi/10.1021/acs.cgd.5c00116.

Phase boundary values, additional crystallization density measurements, crystal size distribution data, a comparison of crystallization densities at varying salt concentrations, time and angular dependence of the dynamic light scattering (DLS) correlation functions (PDF)

## ■ AUTHOR INFORMATION


### Corresponding Author

**Frank Schreiber** − *Institut für Angewandte Physik, Universität Tübingen, 72076 Tübingen, Germany; Center for Light-Matter Interaction, Sensors & Analytics LISA+, 72076 Tübingen, Germany;* orcid.org/0000-0003-3659-6718; Email: frank.schreiber@uni-tuebingen.de

### Authors

**Hadra Banks** − *Institut für Angewandte Physik, Universität Tübingen, 72076 Tübingen, Germany;* orcid.org/0000-0003-1552-8142

**Christian Beck** − *Institut Laue Langevin, Grenoble 38042, France;* orcid.org/0000-0001-7214-3447

**Cara Buchholz** − *Institut für Angewandte Physik, Universität Tübingen, 72076 Tübingen, Germany*

**Simon Christmann** − *Institut für Angewandte Physik, Universität Tübingen, 72076 Tübingen, Germany*

**Furio Surfaro** − *Institut für Angewandte Physik, Universität Tübingen, 72076 Tübingen, Germany*

**Alexander Gerlach** − *Institut für Angewandte Physik, Universität Tübingen, 72076 Tübingen, Germany;* orcid.org/0000-0003-1787-1868

Complete contact information is available at: https://pubs.acs.org/10.1021/acs.cgd.5c00116


### Notes

The authors declare no competing financial interest.

## ■ ACKNOWLEDGMENTS

The authors gratefully acknowledge funding by the DFG (Deutsche Forschungsgemeinschaft). They acknowledge Dr. Robert Jacobs and Dr. Maximilian Skoda for their assistance in the QCM-D experiments. The authors acknowledge Maximilian D. Senft for his valuable comments.

## ■ REFERENCES


(1) Nanev, C. N. Advancements (and challenges) in the study of protein crystal nucleation and growth; thermodynamic and kinetic explanations and comparison with small-molecule crystallization. *Prog. Cryst. Growth Charact. Mater.* **2020**, *66*, No. 100484.

(2) Angkawinitwong, U.; Sharma, G.; Khaw, P. T.; Brocchini, S.; Williams, G. R. Solid-state protein formulations. *Ther. Delivery* **2015**, *6*, 59.

(3) Parker, M. W. Protein structure from X-ray diffraction. *J. Biol. Phys.* **2003**, *29*, 341.

(4) Smyth, M. S.; Martin, J. H. X-ray crystallography. *Mol. Pathol.* **2000**, *53*, 8.

(5) Fankuchen, I. *Advances in Protein*; Anson, M. L.; Edsall, J. T., Eds.; Academic Press, 1945; Vol. 2, p 387.

(6) Gawas, U. B.; Mandrekar, V. K.; Majik, M. S. *Advances in Biological Science*; Meena, S. N.; Naik, M. M., Eds.; Academic Press, 2019; p 69.

(7) Nanev, C. N. On the Molecular Kinetics of Protein Crystal Nucleation and the Causes of Its Slowness: Peculiarities of the Protein−Protein Association. *Crystals* **2025**, *15*, 332.

(8) Whitelam, S.; Dahal, Y. R.; Schmit, J. D. Minimal physical requirements for crystal growth self-poisoning. *J. Chem. Phys.* **2016**, *144*, No. 064903.

(9) Schmit, J. D.; Dill, K. A. Growth rates of protein crystals. *J. Am. Chem. Soc.* **2012**, *134*, 3934.

(10) Beck, C.; Grimaldo, M.; Braun, M. K.; Bühl, L.; Matsarskaia, O.; Jalarvo, N. H.; Zhang, F.; Roosen-Runge, F.; Schreiber, F.; Seydel, T. Temperature and salt controlled tuning of protein clusters. *Soft Matter* **2021**, *17*, 8506.

(11) Zhang, F.; Feustel, M. K.; Skoda, M. W. A.; Jacobs, R. M. J.; Roosen-Runge, F.; Seydel, T.; Sztucki, M.; Schreiber, F. Effective interactions in protein solutions with and without clustering. *Phys. A* **2024**, *650*, No. 129995.

(12) Zhang, F.; Roosen-Runge, F.; Sauter, A.; Wolf, M.; Jacobs, R. M. J.; Schreiber, F. Reentrant condensation, liquid-liquid phase separation and crystallization in protein solutions induced by multivalent metal ions. *Pure Appl. Chem.* **2014**, *86*, 191.

(13) Yang, H.; Yang, S.; Kong, J.; Dong, A.; Yu, S. Obtaining information about protein secondary structures in aqueous solution using Fourier transform IR spectroscopy. *Nat. Protoc.* **2015**, *10*, 382.

(14) Pleitez, M. A.; Khan, A. A.; Soldà, A.; Chmyrov, A.; Reber, J.; Gasparin, F.; Seeger, M. R.; Schätz, B.; Herzig, S.; Scheideler, M.; Ntziachristos, V. Label-free metabolic imaging by mid-infrared optoacoustic microscopy in living cells. *Nat. Biotechnol.* **2020**, *38*, 293.

(15) Giubertoni, G.; Bonn, M.; Woutersen, S. $D_2O$ as an imperfect replacement for $H_2O$: Problem or opportunity for protein research? *J. Phys. Chem. B* **2023**, *127*, 8086.

(16) Broutin, I.; Ries-Kautt, M.; Ducruix, A. Lysozyme solubility in $H_2O$ and $D_2O$ solutions as a function of sodium chloride concentration. *J. Appl. Crystallogr.* **1995**, *28*, 614.

(17) Bucciarelli, S.; Mahmoudi, N.; Casal-Dujat, L.; Jéhannin, M.; Jud, C.; Stradner, A. Extended law of corresponding states applied to solvent isotope effect on a globular protein. *J. Phys. Chem. Lett.* **2016**, *7*, 1610.

(18) Braun, M. K.; Wolf, M.; Matsarskaia, O.; Da Vela, S.; Roosen-Runge, F.; Sztucki, M.; Roth, R.; Zhang, F.; Schreiber, F. Strong isotope effects on effective interactions and phase behavior in protein solutions in the presence of multivalent ions. *J. Phys. Chem. B* **2017**, *121*, 1731.

(19) Tempra, C.; Chamorro, V. C.; Jungwirth, P. Effects of water deuteration on thermodynamic and structural properties of proteins and biomembranes. *J. Phys. Chem. B* **2023**, *127*, 1138.

(20) Fu, L.; Villette, S.; Petoud, S.; Fernandez-Alonso, F.; Saboungi, M.-L. H/D isotope effects in protein thermal denaturation: the case of bovine serum albumin. *J. Phys. Chem. B* **2011**, *115*, 1881.

(21) Reslan, M.; Kayser, V. The effect of deuterium oxide on the conformational stability and aggregation of bovine serum albumin. *Pharm. Dev. Technol.* **2018**, *23*, 1030.

(22) Barbosa, L. R.; Ortore, M. G.; Spinozzi, F.; Mariani, P.; Bernstorff, S.; Itri, R. The importance of protein-protein interactions on the pH-induced conformational changes of bovine serum albumin: a small-angle X-ray scattering study. *Biophys. J.* **2010**, *98*, 147.

(23) Carter, D. C.; Ho, J. X. *Advances in Protein*; Anfinsen, C. B.; Edsall, J. T.; Richards, F. M.; Eisenberg, D. S., Eds.; Academic Press, 1994; Vol. 45, p 153.

(24) Roosen-Runge, F.; Zhang, F.; Schreiber, F.; Roth, R. Ion-activated attractive patches as a mechanism for controlled protein interactions. *Sci. Rep.* **2014**, *4*, No. 7016.

(25) Surfaro, F.; Zhang, F.; Schreiber, F.; Roth, R. The ion-activated attractive patchy particle model and its application to the liquid-vapor phase transitions. *J. Chem. Phys.* **2024**, *161*, No. 034901.

(26) Maier, R.; Fries, M. R.; Buchholz, C.; Zhang, F.; Schreiber, F. Human versus Bovine Serum Albumin: A subtle difference in hydrophobicity leads to large differences in bulk and interface behavior. *Cryst. Growth Des.* **2021**, *21*, 5451.

(27) Maier, R.; Zocher, G.; Sauter, A.; Da Vela, S.; Matsarskaia, O.; Schweins, R.; Sztucki, M.; Zhang, F.; Stehle, T.; Schreiber, F. Protein crystallization in the presence of a metastable liquid-liquid phase separation. *Cryst. Growth Des.* **2020**, *20*, 7951.
(28) Buchholz, C.; Reichart, L. F.; Surfaro, F.; Maier, R.; Zhang, F.; Gerlach, A.; Schreiber, F. Kinetics of HSA crystallization and its relationship with the phase diagram. *J. Cryst. Growth* **2023**, *603*, No. 126959.
(29) Matsarskaia, O.; Roosen-Runge, F.; Schreiber, F. Multivalent ions and biomolecules: Attempting a comprehensive perspective. *ChemPhysChem* **2020**, *21*, 1742.
(30) Fries, M. R.; Stopper, D.; Skoda, M. W. A.; Blum, M.; Kertzscher, C.; Hinderhofer, A.; Zhang, F.; Jacobs, R. M. J.; Roth, R.; Schreiber, F. Enhanced protein adsorption upon bulk phase separation. *Sci. Rep.* **2020**, *10*, No. 10349.
(31) Fries, M. R.; Conzelmann, N. F.; Günter, L.; Matsarskaia, O.; Skoda, M. W. A.; Jacobs, R. M. J.; Zhang, F.; Schreiber, F. Bulk phase behavior vs interface adsorption: Specific multivalent cation and anion effects on BSA interactions. *Langmuir* **2021**, *37*, 139.
(32) Senft, M. D.; Zocher, G.; Retzbach, S.; Maier, R.; Hiremath, A.; Zhang, F.; Stehle, T.; Schreiber, F. Role of Specific and Nonspecific Interactions in the Crystallization Behavior of BSA and HSA Protein Solutions. *Cryst. Growth Des.* **2025**, *25*, 2418.
(33) Banks, H.; Surfaro, F.; Pastryk, K.-F.; Buchholz, C.; Zaluzhnyy, I. A.; Gerlach, A.; Schreiber, F. From adsorption to crystallization of proteins: Evidence for interface-assisted nucleation. *Colloids Surf., B* **2024**, *241*, No. 114063.
(34) Fries, M. R.; Skoda, M. W. A.; Conzelmann, N. F.; Jacobs, R. M. J.; Maier, R.; Scheffczyk, N.; Zhang, F.; Schreiber, F. Bulk phase behaviour vs interface adsorption: Effects of anions and isotopes on $\beta$-lactoglobulin (BLG) interactions. *J. Colloid Interface Sci.* **2021**, *598*, 430.
(35) Quinlan, G. J.; Martin, G. S.; Evans, T. W. Albumin: Biochemical properties and therapeutic potential. *Hepatology* **2005**, *41*, 1211.
(36) Surfaro, F.; Maier, R.; Pastryk, K.-F.; Zhang, F.; Schreiber, F.; Roth, R. An alternative approach to the osmotic second virial coefficient of protein solutions and its application to liquid-liquid phase separation. *J. Chem. Phys.* **2023**, *158*, No. 164902.
(37) Beck, C.; Mosca, I.; Miñarro, L. M.; et al. A multiscale in situ time-resolved study of the nano- to millisecond structural dynamics during protein crystallization. *J. Appl. Crystallogr.* **2025**, *58*, 845.
(38) Nanev, C. N.; Tonchev, V. D. Sigmoid kinetics of protein crystal nucleation. *J. Cryst. Growth* **2015**, *427*, 48.
(39) Hardy, R. C.; Cottington, R. L. Viscosity of Deuterium Oxide and Water from 5° to 125°C. *J. Chem. Phys.* **1949**, *17*, 509.
(40) Sohna Sohna, J. E.; Cooper, M. A. Does the Sauerbrey equation hold true for binding of peptides and globular proteins to a QCM?: A systematic study of mass dependence of peptide and protein binding with a piezoelectric sensor. *Sens. Bio-Sens. Res.* **2016**, *11*, 71.
(41) Easley, A. D.; Ma, T.; Eneh, C. I.; Yun, J.; Thakur, R. M.; Lutkenhaus, J. L. A practical guide to quartz crystal microbalance with dissipation monitoring of thin polymer films. *J. Polym. Sci.* **2022**, *60*, 1090.
(42) Feiler, A. A.; Sahlholm, A.; Sandberg, T.; Caldwell, K. D. Adsorption and viscoelastic properties of fractionated mucin (BSM) and bovine serum albumin (BSA) studied with quartz crystal microbalance (QCM-D). *J. Colloid Interface Sci.* **2007**, *315*, 475.
(43) van der Westen, R.; Sharma, P. K.; De Raedt, H.; Vermue, I.; van der Mei, H. C.; Busscher, H. J. Elastic and viscous bond components in the adhesion of colloidal particles and fibrillated streptococci to QCM-D crystal surfaces with different hydrophobicities using Kelvin-Voigt and Maxwell models. *Phys. Chem. Chem. Phys.* **2017**, *19*, 25391.
(44) Voinova, M. V.; Rodahl, M.; Jonson, M.; Kasemo, B. Viscoelastic acoustic response of layered polymer films at fluid-solid interfaces: Continuum mechanics approach. *Phys. Scr.* **1999**, *59*, No. 391.
(45) Liu, S. X.; Kim, J.-T. Application of KelvinVoigt model in quantifying whey protein adsorption on polyethersulfone using QCM-D. *J. Lab. Autom.* **2009**, *14*, 213.
(46) Grimaldo, M.; Roosen-Runge, F.; Hennig, M.; Zanini, F.; Zhang, F.; Zamponi, M.; Jalarvo, N.; Schreiber, F.; Seydel, T. Salt-induced universal slowing down of the short-time self-diffusion of a globular protein in aqueous solution. *J. Phys. Chem. Lett.* **2015**, *6*, 2577.
(47) Soraruf, D.; Roosen-Runge, F.; Grimaldo, M.; Zanini, F.; Schweins, R.; Seydel, T.; Zhang, F.; Roth, R.; Oettel, M.; Schreiber, F. Protein cluster formation in aqueous solution in the presence of multivalent metal ions - a light scattering study. *Soft Matter* **2014**, *10*, 894−902.
(48) Mosca, I.; Beck, C.; Jalarvo, N. H.; Matsarskaia, O.; Roosen-Runge, F.; Schreiber, F.; Seydel, T. Continuity of Short-Time Dynamics Crossing the Liquid-Liquid Phase Separation in Charge-Tuned Protein Solutions. *J. Phys. Chem. Lett.* **2024**, *15*, 12051.
(49) Tokuyama, M.; Oppenheim, I. Dynamics of hard-sphere suspensions. *Phys. Rev. E* **1994**, *50*, No. R16.
(50) Beck, C.; Grimaldo, M.; Roosen-Runge, F.; Maier, R.; Matsarskaia, O.; Braun, M.; Sohmen, B.; Czakkel, O.; Schweins, R.; Zhang, F.; Seydel, T.; Schreiber, F. Following protein dynamics in real time during crystallization. *Cryst. Growth Des.* **2019**, *19*, 7036−7045.
(51) Chun, S. Y.; Son, M. K.; Park, C. R.; Lim, C.; Kim, H. I.; Kwak, K.; Cho, M. Direct observation of protein structural transitions through entire amyloid aggregation processes in water using 2D-IR spectroscopy. *Chem. Sci.* **2022**, *13*, 4482.
(52) Pathak, A. K.; Bandyopadhyay, T. Water isotope effect on the thermostability of a polio viral RNA hairpin: A metadynamics study. *J. Chem. Phys.* **2017**, *146*, No. 165104.
(53) Mizuno, K.; Bächinger, H. P. The effect of deuterium oxide on the stability of the collagen model peptides H-(Pro-Pro-Gly)$_{10}$-OH, H-(Gly-Pro-4(R)Hyp)$_9$-OH, and Type I collagen. *Biopolymers* **2010**, *93*, 93.
(54) Rabe, M.; Verdes, D.; Seeger, S. Understanding protein adsorption phenomena at solid surfaces. *Adv. Colloid Interface Sci.* **2011**, *162*, 87.
(55) Fair, B. D.; Jamieson, A. M. Studies of protein adsorption on polystyrene latex surfaces. *J. Colloid Interface Sci.* **1980**, *77*, 525.
(56) Guo, B.; Kao, S.; McDonald, H.; Asanov, A.; Combs, L. L.; Wilson, W. W. Correlation of second virial coefficients and solubilities useful in protein crystal growth. *J. Cryst. Growth* **1999**, *196*, 424.
(57) Gripon, C.; Legrand, L.; Rosenman, I.; Vidal, O.; Robert, M. C.; Boué, F. Lysozyme-lysozyme interactions in under- and supersaturated solutions: a simple relation between the second virial coefficients in $H_2O$ and $D_2O$. *J. Cryst. Growth* **1997**, *178*, 575.
(58) Guo, Y.-Z.; Sun, L. H.; Oberthuer, D.; et al. Utilisation of adsorption and desorption for simultaneously improving protein crystallisation success rate and crystal quality. *Sci. Rep.* **2014**, *4*, No. 7308.
(59) Xu, D.; Tsai, C. J.; Nussinov, R. Hydrogen bonds and salt bridges across protein-protein interfaces. *Protein Eng.* **1997**, *10*, 999.
(60) Rudolph, W. W.; Irmer, G. Hydration and ion pair formation in common aqueous La(III) salt solutions - a Raman scattering and DFT study. *Dalton Trans.* **2015**, *44*, 295.
(61) Roosen-Runge, F.; Heck, B. S.; Zhang, F.; Kohlbacher, O.; Schreiber, F. Interplay of pH and binding of multivalent metal ions: Charge inversion and reentrant condensation in protein solutions. *J. Phys. Chem. B* **2013**, *117*, 5777.


https://doi.org/10.1021/acs.cgd.5c00116
*Cryst. Growth Des.* 2025, 25, 5174−5182